J of Astronaut Sci (2018) 65:111–134
DOI 10.1007/s40295-017-0114-8

An Unscented Kalman-Particle Hybrid Filter for Space Object Tracking

Dilshad Raihan A.V[1] **· Suman Chakravorty**[1]

Published online: 13 April 2017

Abstract Optimal and consistent estimation of the state of space objects is pivotal to surveillance and tracking applications. However, probabilistic estimation of space objects is made difficult by the non-Gaussianity and nonlinearity associated with orbital mechanics. In this paper, we present an unscented Kalman-particle hybrid filtering framework for recursive Bayesian estimation of space objects. The hybrid filtering scheme is designed to provide accurate and consistent estimates when measurements are sparse without incurring a large computational cost. It employs an unscented Kalman filter (UKF) for estimation when measurements are available. When the target is outside the field of view (FOV) of the sensor, it updates the state probability density function (PDF) via a sequential Monte Carlo method. The hybrid filter addresses the problem of particle depletion through a suitably designed filter transition scheme. To assess the performance of the hybrid filtering approach, we consider two test cases of space objects that are assumed to undergo full three dimensional orbital motion under the effects of J_2 and atmospheric drag perturbations. It is demonstrated that the hybrid filters can furnish fast, accurate and consistent estimates outperforming standard UKF and particle filter (PF) implementations.

Keywords Space object tracking · Nonlinear filtering · Curse of dimensionality · Sequential Monte Carlo methods · Uncertainty propagation · Space situational awareness

This work is funded by AFOSR grant number: FA9550-13-1-0074 under the Dynamic Data Driven Application Systems (DDDAS) program.

✉ Dilshad Raihan A.V
dilshadraihan@tamu.edu

[1] Texas A&M University, College Station, TX, USA

Introduction

Probabilistic estimation of the state of space objects is a problem of substantial interest in many fields such as tracking and surveillance. A great volume of prior research is available on the design of optimal and suboptimal estimators for probabilistic inference in stochastic dynamical systems. The optimal linear estimator, known as the Kalman filter, set the framework for recursive estimation of uncertain dynamical systems using state space description [14, 15]. The Kalman filter furnishes the unbiased minimum variance estimates when the dynamical system is linear and the uncertainties involved are Gaussian. However the dynamics of space objects is governed by forces, such as the Newtonian gravitation, that involve nonlinear functions of state variables. The development of the extended Kalman filter (EKF) set forth the attempts to derive an optimal filter for nonlinear dynamical systems [6, 19, 21]. The EKF involves linearization of the state transition equations and the observation model at the current estimated state. It enforces several restrictive assumptions on the system and accumulates linearization errors. The emergence of sigma point Kalman filters, specifically the UKF, gave rise to a derivative free alternative to the EKF [12, 13, 24]. The UKF computes the statistics of the state PDF using carefully chosen and weighted sigma points. It was found to consistently outperform the EKF at a comparable computational cost. However, as the UKF approximates the statistics of the posterior PDF using the first two moments, it can be ineffective in the estimation of a general multimodal non-Gaussian PDF. Handling the non-Gaussianity of the state PDF is crucial to space object tracking as the measurements may be sparse and the PDF may undergo extensive distortion induced by nonlinearities. In such cases, the UKF may even produce suboptimal and diverging estimates [17].

The particle filter (PF) is a sequential Monte Carlo estimator which employs a suitably large number of particles, constituting a representative ensemble of the state PDF, for state estimation. It is a robust nonlinear estimator since it does not make any restrictive assumption about the nature of the PDF or dynamics [2, 11]. It has been proved that the variance of the particle weights is a nondecreasing function of time [9]. Consequently, over a few time steps, the sample would encounter weight depletion, wherein a large section of the particles would retain only negligible weights. Weight degeneration is undesirable and it can be countered by employing a large enough sample of particles. However, the number of particles required to prevent weight depletion increases exponentially as the dimension of the state space is increased [4]. As a result, PF implementations are often computationally expensive [7]. Estimation of nonlinear dynamical systems by employing a Gaussian mixture model (GMM) to approximate the state PDF has also been proposed [1, 22]. Methods to improve the accuracy of GMM filters by updating the mixture modes between measurements have garnered much attention recently [8, 23]. However, these approaches require frequent optimization operations or entropy calculations during the propagation stage.

The ensemble Kalman filter (EnKF) is a nonlinear estimation scheme mainly employed in the estimation of extremely large order dynamical systems [10, 25]. Originally developed as an alternative to the EKF, the EnKF employs an ensemble of

states to capture the error statistics. In the forecast step, a set of states sampled from the prior distribution is substituted in the dynamic model equations to account for the evolution of the system. In the stochastic variant of the EnKF, the data assimilation step involves updating the ensemble via a Kalman gain expression using a perturbed observation ensemble. The perturbations terms, usually drawn from a Gaussian PDF, evolve nonlinearly when the system model is extremely nonlinear or when the time interval between successive measurement updates is too long. The nonlinear evolution of the perturbation terms are known to be detrimental to the performance of EnKF [16].

In this paper, we propose a novel hybrid filtering framework which incorporates select features of both UKF and PF to produce a fast and accurate nonlinear filter that can be employed for space object tracking. When the target is moving within the FOV of the observer, a UKF is used for state estimation as frequent measurements may be available and the growth in uncertainty will be limited. As the target moves out of the FOV, an ensemble of particles is sampled from the state PDF and propagated forward in time using the available model of the orbital dynamics. Since the PF is free from restrictive assumptions on the nature of dynamics and PDF, the between-measurements distortions of the state PDF can be conveniently kept track of in this manner without incurring a large computational cost. However, the problem of weight depletion arises when the object re-enters the FOV of sensor as a new measurement is recorded. This is addressed through a suitably designed PF to UKF transition scheme. We consider three approaches to performing this transition and evaluate their estimation performance. A comparison study has been conducted to assess the performance of the hybrid filters with respect to that of standard UKF and PF implementations. The new filtering scheme is demonstrated to be capable of producing accurate and consistent estimates even in large uncertainty and sparse measurement scenarios.

The remainder of this paper is organized as follows. A brief overview of the space object tracking problem is given in "Problem Statement". Short technical descriptions of the PF and the UKF are provided in "Background". A detailed account of the filter design process is provided in the section titled "The Unscented Kalman-Particle Hybrid Filter". The dynamics of the orbiting objects and an angles-only measurement model are discussed in the section titled "Dynamics & Measurement Models". The hybrid filter is employed in the estimation of two tests cases of LEO objects in the section named "Simulations and Results".

Problem Statement

Consider the dynamical system given by

$$\mathbf{X}_t = f(\mathbf{X}_{t-1}) + \mathbf{w}_t. \tag{1}$$

Here $\mathbf{X}_t$ represents the state vector and $f(\mathbf{X})$ the modeled dynamics. The stochastic term $\mathbf{w}_t$ accounts for the effect of modeling uncertainties and external noise. Assume

that we obtain measurements at discrete times t to aid the estimation of the system. The measurement process may be expressed as

$$\mathbf{z}_t = g(\mathbf{X}_t) + \boldsymbol{\nu}_t, \tag{2}$$

where $\boldsymbol{\nu}_t$ represents the measurement noise. Given the dynamic and measurement models, a tracking scheme attempts to estimate the state of the dynamical system conditioned on the measurements. The primary objective of this work in particular is to design a tracking scheme that is capable of estimating the conditional state PDF $p(\mathbf{X}_t|\mathbf{Z}_t)$ of a space object accurately and consistently, given the initial state PDF $p(\mathbf{X}_0)$ and the dynamic and measurement models. Here $\mathbf{Z}_t$ represents the sequence of all measurements recorded until time t.

When the statistics of the process noise $\mathbf{w}_t$ and measurement noise $\boldsymbol{\nu}_t$ are known, the transition density function $p(\mathbf{X}_{t+1}|\mathbf{X}_t)$ and the measurement likelihood function $P(\mathbf{z}_t|\mathbf{X}_t)$ can be computed in a straightforward fashion. When these two functions are available, the required filtered density $p(\mathbf{X}_t|\mathbf{Z}_t)$ may be computed in a recursive manner that involves two basic steps. In the first step, the predicted density of the state at time $t+1$ conditioned on $\mathbf{Z}_t$ is computed using the Chapman-Kolmogorov equation as

$$p(\mathbf{X}_{t+1}|\mathbf{Z}_t) = \int p(\mathbf{X}_{t+1}|\mathbf{X}_t)\, p(\mathbf{X}_t|\mathbf{Z}_t) d\mathbf{X}_t. \tag{3}$$

Let $\mathbf{z}_{t+1}$ be the measurement vector recorded at time $t+1$. The second step known as the update step involves computing the posterior PDF $p(\mathbf{X}_{t+1}|\mathbf{z}_{t+1}, \mathbf{Z}_t)$ according to the Bayes' rule as

$$p(\mathbf{X}_{t+1}|\mathbf{Z}_{t+1}) = \frac{p(\mathbf{z}_{t+1}|\mathbf{X}_{t+1})\, p(\mathbf{X}_{t+1}|\mathbf{Z}_t)}{\int p(\mathbf{z}_{t+1}|\mathbf{X}')\, p(\mathbf{X}'|\mathbf{Z}_t) d\mathbf{X}'}. \tag{4}$$

When the process and measurement models are linear and the random variables $\mathbf{X}_0$, $\mathbf{w}_t$ and $\boldsymbol{\nu}_t$ are normally distributed, the predicted and updated densities are guaranteed to be normally distributed at all time instants. This greatly simplifies the estimation of linear systems that are perturbed by additive Gaussian noise. However, if the transformation functions are nonlinear, then the random variable $\mathbf{X}_{t+1}$ may be distributed according to complex non-Gaussian densities. Computing an exact analytic expression for $p(\mathbf{X}_{t+1}|\mathbf{Z}_{t+1})$ can be extremely difficult in such cases. As the forces affecting the time evolution of the space objects are mostly nonlinear, space object tracking is a nonlinear filtering problem. Most nonlinear filtering algorithms that have hitherto been proposed rely on various approximation techniques, for e.g. linearizing the transformation functions, to perform the propagation and update steps. Additionally, the state PDF is often approximated to be a unimodal Gaussian PDF to facilitate the implementation of fast Kalman filter like algorithms. However, there are several aspects of the space object tracking problem that limit the applicability of these approximation techniques. For e.g., the total number of measurements that can be recorded over a fixed time period is limited by the number and cost of sensors and the area of sky that they can scan, i.e., their field of view (FOV). Hence the measurements can often be infrequent. In such a case, the state PDF may undergo extensive nonlinearity induced distortion along the orbit and the Gaussian approximation may not be valid. The dimensionality of the space object tracking problem can also prove

to be an impediment. A complete representation of the state of a space object in three dimensional motion requires six coordinates. However, it has been observed that some of the most commonly used filtering algorithms have only limited success in dimensions greater than three due to computational limitations. It is important for any estimator designed to perform space object tracking to address these three factors, i.e., the nonlinearity, dimensionality and sparsity of measurements.

In addition to the three factors mentioned above we make the following observation regarding the uncertainty propagation in orbital systems that is relevant to the design of an efficient and robust filter.

1. *S*ensitivity with respect to uncertainty in velocity: The growth in uncertainty with time is remarkably sensitive towards initial error in velocity. Since the mechanical energy of the space object varies as the square of the velocity, increasing the uncertainty in velocity leads to larger variations in mechanical energy. This manifests as an increased uncertainty in the length of semimajor axis. Consequently, a lower initial uncertainty in velocity helps to keep the trajectories closer together resulting in a much slower growth in uncertainty.

Background

In this section, we briefly overview two nonlinear filtering techniques that are particularly relevant to the present work.

1. *Particle Filters*: Particle filters rely on a weighted ensemble of state vectors called the particles to approximate the state PDF [2, 11]. The particles and their weights $\{\mathbf{X}_t^i, \mathbf{w}_t^i\}$ define a Dirac delta representation of the state PDF as given by

$$p(\mathbf{X}_t|\mathbf{Z}_t) \approx \sum_{i=1}^{N} \mathbf{w}_t^i \delta(\mathbf{X}_t - \mathbf{X}_t^i). \tag{5}$$

An ensemble representation of the joint posterior $p(\mathbf{X}_{1:t}|\mathbf{Z}_t)$ can be obtained using the importance sampling technique as follows. Initially the particles $\mathbf{X}_{1:t}^i$ are drawn from a known importance function $q(\mathbf{X}_{1:t}|\mathbf{Z}_t)$. To construct a sample from the PDF $p(\mathbf{X}_{1:t}|\mathbf{Z}_t)$, each particle $\mathbf{X}_{1:t}^i$ is then assigned a weight $\mathbf{w}_t^i$ so that

$$\mathbf{w}_t^i \propto \frac{p(\mathbf{X}_{1:t}^i|\mathbf{Z}_t)}{q(\mathbf{X}_{1:t}^i|\mathbf{Z}_t)}, \tag{6}$$

$$\sum_{i=1}^{N} \mathbf{w}_t^i = 1. \tag{7}$$

Given this ensemble, a particle representation of $p(\mathbf{X}_t|\mathbf{Z}_{1:t})$ can be obtained by marginalizing the Dirac delta representation over $\mathbf{X}_{1:t-1}$. Given an ensemble representation $\{\mathbf{X}_{1:t}^i, w_t^i\}$ of $p(\mathbf{X}_{1:t}|\mathbf{Z}_t)$ and an importance function that satisfies

$$q(\mathbf{X}_{1:t+1}|\mathbf{Z}_{t+1}) = q(\mathbf{X}_{t+1}|\mathbf{X}_t, \mathbf{z}_{t+1}) q(\mathbf{X}_{1:t}|\mathbf{Z}_t) \tag{8}$$

we can generate an ensemble from $p(\mathbf{X}_{1:t+1}|\mathbf{Z}_{t+1})$ by sampling $\mathbf{X}^i_{t+1}$ from $q(\mathbf{X}_{t+1}|\mathbf{X}^i_t, z_{t+1})$ and then combining it with $\mathbf{X}^i_{1:t}$. The new weights $\mathbf{w}^i_{t+1}$ are then proportional to

$$\mathbf{w}^i_{t+1} \propto \frac{p(\mathbf{z}_{t+1}|\mathbf{X}_{t+1})p(\mathbf{X}_{t+1}|\mathbf{X}_t)\mathbf{w}^i_t}{q(\mathbf{X}_{t+1}|\mathbf{X}_t, \mathbf{Z}_t)}. \tag{9}$$

Choosing $q(\mathbf{X}_{t+1}|\mathbf{X}_t) = p(\mathbf{X}_{t+1}|\mathbf{X}_t)$ allows the ensemble $\mathbf{X}^i_{t+1}$ to be drawn by propagating $\mathbf{X}^i_t$ using the dynamic model. The weights are then multiplied by a factor proportional to $p(\mathbf{z}_{t+1}|\mathbf{X}_{t+1})$. The main drawback of particle filters is a phenomenon known as weight depletion wherein all but a few particles get negligible weights. This leads to underestimating the uncertainty. This is a major setback to estimation in higher dimensions as depletion gets increasingly more likely in large dimensions. Preventing weight depletion requires the number of particles to be increased exponentially with the dimension of the state space.

2. *Unscented Kalman Filters*: The UKF is a Kalman like filter that employs the unscented transform (UT) to perform the propagation and update steps. The unscented transform is a widely used method for computing the statistics of random variables undergoing nonlinear transformations. The PDF of the random variable is approximated by a set of carefully chosen points namely the sigma points. In order to compute the statistics of the transformed variable, the nonlinear transformation is applied to the sigma points individually. Any set of points that can capture the mean and covariance of the original PDF may be used as sigma points. In practice, they are deterministically chosen and weighted so that any available information of higher order moments may be incorporated as well [12]. A frequently administered choice of the sigma point set consists of the mean of the random variable of dimension n, along with a collection of $2n$ points that lie symmetrically on a contour ellipse of its covariance. Given a random variable X with mean μ and covariance C, the sigma points are chosen as

$$\begin{aligned}
\chi_0 &= \hat{\mu} \\
\chi_i &= \hat{\mu} + \left(\sqrt{(n+\lambda)\,C}\right)_i \quad i = 1, \ldots, n \\
\chi_i &= \hat{\mu} - \left(\sqrt{(n+\lambda)\,C}\right)_i \quad i = n+1, \ldots, 2n.
\end{aligned} \tag{10}$$

Here, λ is a scaling parameter that is chosen to determine the spread of sigma points about μ. The term $\left(\sqrt{(n+\lambda)C}\right)_i$ represents the i-th row of the matrix square root. The sigma points χ_i are assigned weights such that $w_i = \frac{1}{2(n+\lambda)}$ when $i \neq 0$ and $\sum_{i=0}^{2n+1} w_i = 1$. Given the sigma points and their weights, the expectation of a nonlinear function of X, $y = f(X)$ can be approximated as

$$E(y) \approx \sum_{i=0}^{2n} w_i f(\chi_i). \tag{11}$$

The UKF estimates the first two moments of the state random variable using UT. However, the first two moments can often prove inadequate in describing a random

variable unless it is normally distributed. A step by step description of the UKF computations can be found in [24].

The Unscented Kalman-Particle Hybrid Filter

In this section we discuss the UKF-PF hybrid filtering approach to space object tracking. Before proceeding further we state two key assumptions

Assumption 1 *We shall assume that the filtered state PDF of the object while inside the FOV can be well approximated by a unimodal PDF.*

This may not be a bad assumption given that frequent disambiguating measurements are recorded when the space object is within the FOV of the sensor.

The orbital perturbations that influence the dynamics of space objects are well known. Consequently, accurate computational models that can simulate the time evolution of space objects are available. Employing an accurate model helps to minimize the variations due to differences between modeled and actual dynamics. We also assume that high precision models that limit the statistical variability in the time evolution of the space object are available. Based on these observations we make the following assumption.

Assumption 2 *We assume that the magnitude of process noise affecting the dynamics of the space object is minimal.*

We shall now discuss the UKF-PF hybrid filtering approach in detail. The hybrid filtering approach presented here is formulated on the basic premise that a carefully chosen combination of multiple approximation schemes may accord a higher overall estimation performance than any one particular scheme, owing to the high specificity of individual schemes' performance to the estimation scenario under study. In particular, the UKF-PF hybrid filter proposes to employ a particle approximation of the state PDF when the space object is outside the FOV of sensors and to switch to a unimodal approximation when the object is inside the observation range. The approximate unimodal PDF is characterized by a mean and covariance. The rationale behind this particular selection of approximation methods is discussed below.

As mentioned previously, when the space object is outside the observation range, the state PDF undergoes extensive nonlinearity induced distortion. In the absence of measurements, particles from the PDF at time $t+1$, i.e., $p(\mathbf{X}_{t+1}|\mathbf{Z}_t)$, may be obtained by merely propagating the ensemble at time t through the dynamic model as this is equivalent to choosing $q(\mathbf{X}_{t+1}|\mathbf{X}_t) = p(\mathbf{X}_{t+1}|\mathbf{X}_t)$. This is a key advantage of the particle approximation as the Dirac delta kernels are allowed to freely evolve with time without enforcing any restrictive assumptions on the nature of state PDF. Moreover, by increasing the number of particles, the approximation may by refined to any degree of accuracy. Additionally, particle based methods do not require any auxiliary optimization or entropy calculations to incorporate the effects of distortions. This makes the particle approach well suited for keeping track of the evolution of state

PDF when the object is outside the observation range. Moreover, as no measurement update is performed outside the FOV, the sample weights remain constant. Hence, the particle based estimator can be employed outside the FOV without facing the prospect of particle depletion and the associated curse of dimensionality. As a result, a tracking scheme that employs a particle approximation only during the flight of the object outside the FOV can use a much smaller number of particles in comparison to a full PF implementation.

Availability of frequent measurements during the flight of the object inside the FOV ensures that the growth and distortion of uncertainty between consecutive measurements will be limited. The hybrid filter employs a unimodal Gaussian density to approximate the state PDF during this stage. The expectation integrals involved in the calculation of mean and covariance of the propagated state can be evaluated using the unscented transform (UT). These are then used to fit a Gaussian PDF for the propagated PDF. The measurement update step in a standard UKF is free from resampling procedures that are customary to sequential Monte Carlo methods. As the propagated PDF and measurement random variable are assumed to be Gaussian, the UKF employs a Kalman measurement update to compute the mean and covariance of the posterior PDF. The UKF measurement update resembles the linear minimum variance update that appears in the Kalman Filter. The Kalman gain K_k that is used to update the estimate is computed as $K_k = C_{XZ}C_{ZZ}^{-1}$. The covariance C_{ZZ} and cross covariance C_{XZ} can also be computed using UT. Additionally,the standard UT uses only $2n + 1$ sample points for evaluating the integrals in an n-dimensional estimation problem. The minimum number of points required by the UT to match the mean and covariance of an n-dimensional random variable is only $n + 1$. Hence it is computationally efficient. The sequencing of filters that underlies the UKF-PF hybrid estimator is illustrated in Fig. 1.

In practice, when the estimated position of the object exits the FOV of the sensor, we sample a set of equally weighted particles from the unimodal Gaussian state PDF. Subsequently, they are propagated forward in time while maintaining the individual

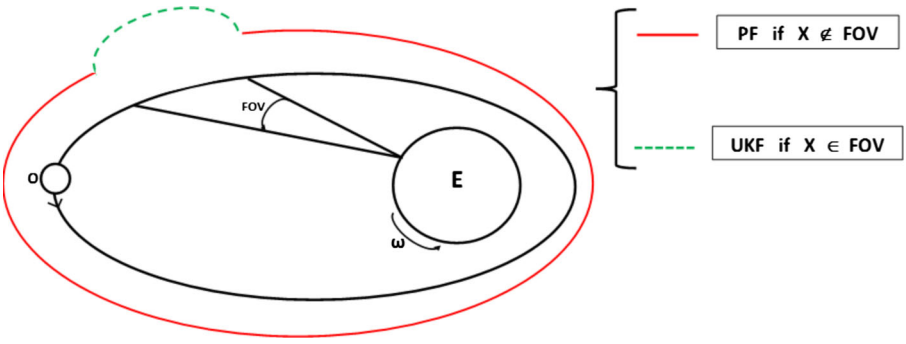

Fig. 1 The hybrid approach attempts to harness the merits of both PF and UKF

particle weights $w(\mathbf{X}^i)$ constant till the reentry of the object into FOV. The hybrid filter switches from the particle set to the unimodal UKF at the re-entry of the object into the sensor's FOV, which is marked by the reappearance of measurements. During this transition, a unimodal density has to be retrieved from the ensemble of particles while incorporating the additional information obtained from the newly recorded measurement. During the operation of the hybrid filter, a measurement update is performed on the particles solely at this PF-UKF transition stage. It needs to be emphasized that as the state space is six dimensional and observations are sparse, the estimator my face a significant risk of particle depletion at this stage. The new measurement information may be incorporated into the state PDF in a number of ways, for e.g. by performing a direct particle measurement update on the ensemble [2]. Alternatively, the posterior mean and covariance may be determined by refining the prior mean and covariance through a Kalman update step [14]. In this study, we have considered three approaches for transitioning from PF to UKF. In hybrid filter 1, the PF-UKF transition is accomplished through a particle measurement update. In hybrid filters 2 and 3, the posterior statistics are computed via a Kalman update. However, the filters 2 and 3 adopt different approaches to computing the Kalman gain. The three transition designs are discussed in detail below.

Hybrid Filter 1

Once the object re-enters the FOV and the first measurement is registered, all N particles are assigned weights based on their respective likelihoods derived from the measurement model. The weight assigned to each particle $\mathbf{X}^i_{t_r}$ at any instant t_r may be computed as

$$w(\mathbf{X}^i_{t_r}) = \frac{p(\mathbf{z}_{t_r}|\mathbf{X}^i_{t_r})}{\sum_{j=1}^{N} p(\mathbf{z}_{t_r}|\mathbf{X}^j_{t_r})}, \tag{12}$$

where $\mathbf{z}_{t_r}$ is the measurement recorded at that instant. The mean (μ_{X,t_r}) and covariance (C_{X,t_r}) of this weighted sample may be computed as

$$\mu_{X,t_r} = \sum_{i=1}^{N} w(\mathbf{X}^i_{t_r})\mathbf{X}^i_{t_r}, \tag{13}$$

$$C_{X,t_r} = \sum_{i=1}^{N} \frac{w(\mathbf{X}^i_{t_r})(\mathbf{X}^i_{t_r} - \boldsymbol{\mu}_{X_{t_r}})(\mathbf{X}^i_{t_r} - \boldsymbol{\mu}_{X_{t_r}})^T}{1 - \Sigma_{j=1}^{N} w(\mathbf{X}^j_{t_r})^2}. \tag{14}$$

The $\mu_{X_{t_r}}$ and $C_{X_{t_r}}$ described in Eqs. 13 and 14 are then used to initialize the approximate unimodal PDF required for the subsequent UKF based estimation.

As mentioned previously, all particles are equally weighted prior to the transition from PF to UKF. Figure 2a shows the distribution of weights of 500 particles before the PF to UKF transition. Since the weights must add up to unity, we find that $w(\mathbf{X}^i_t) = 1/500, \forall i \in [1, 500]$. Once the importance weights are updated with measurement likelihoods, the contribution from several particles to the posterior PDF $p(\mathbf{X}_{t_r}|\mathbf{Z}_{t_r})$ diminishes due to their getting negligible weights. The distribution of

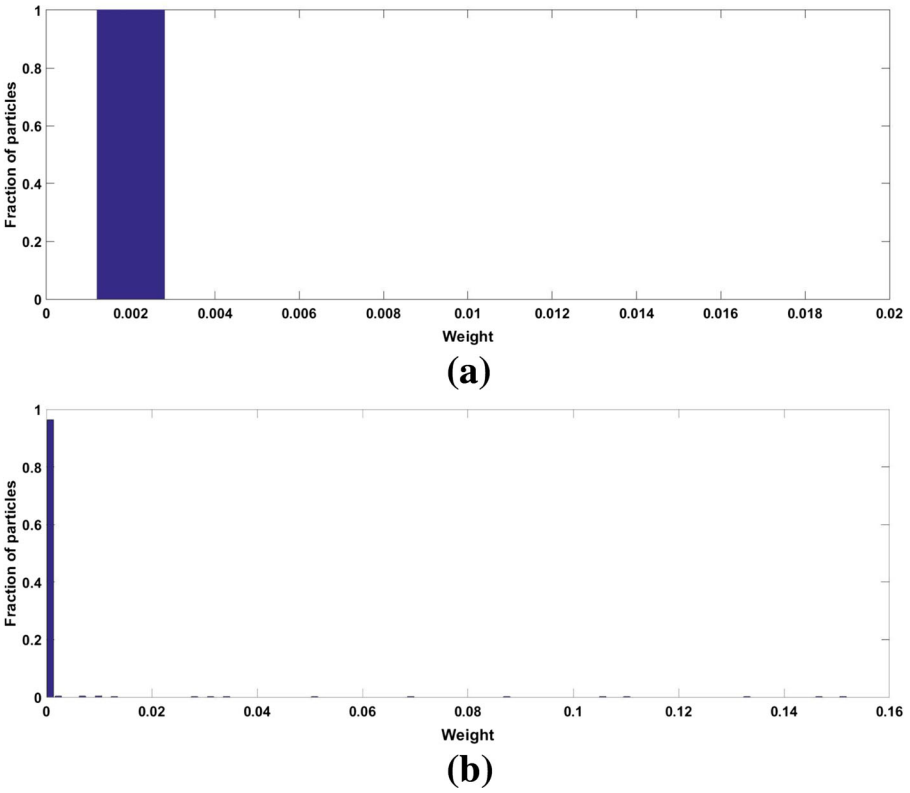

Fig. 2 Distribution of particle weights **a** before PF to UKF transition **b** after PF to UKF transition

particle weights after the measurement update is given in Fig. 2b. Particles with negligible weights are discarded during resampling. The particle measurement update may expose the filter to the risk of weight depletion and covariance collapse, particularly when the sample size is small as a sizable fraction of particles may be presented with negligible likelihoods. Evaluating the measurement likelihoods can be avoided if the measurement update is performed using a Kalman update step.

Hybrid Filter 2

Let t_e be the time at which the space object exits the observation range and $t_r > t_e$ be its time of re-entry. Then the ensemble of particles obtained at time t_r prior to the measurement update is essentially a sample drawn from the propagated state distribution $p(\mathbf{X}_{t_r}|\mathbf{Z}_{t_e})$. Let this ensemble be denoted by $A_{t_r} = \{\mathbf{X}_{t_r}^1, \mathbf{X}_{t_r}^2, \ldots, \mathbf{X}_{t_r}^N\}$ where N represents the total number of particles. Then the mean and covariance of the PDF $p(X_{t_r}|Z_{t_e})$ may be approximated as

$$\begin{aligned} E(\mathbf{X}_{t_r}|\mathbf{Z}_{t_e}) &\approx \hat{\mu}_{A,t_r}, \\ cov(\mathbf{X}_{t_r}|\mathbf{Z}_{t_e}) &\approx \hat{C}_{A,t_r}. \end{aligned} \tag{15}$$

Here $\hat{\mu}_{A,t_r}$ and $\hat{C}_{A,t_r}$ are respectively the sample mean and sample covariance of A_{t_r}. It is then possible to obtain an approximate mean and covariance of the posterior PDF $p(\mathbf{X}_{t_r}|\mathbf{Z}_{t_r})$ by performing a Kalman measurement update on $\hat{\mu}_{A,t_r}$ and $\hat{C}_{A,t_r}$. The posterior state estimate obtained in this manner may then be appropriated for the subsequent UKF based estimation. The detailed steps involved in computing the posterior mean μ_{X,t_r} and covariance C_{X,t_r} are given below:

$$
\begin{aligned}
\hat{\mu}_{A,t_r} &= \frac{1}{N}\sum_{l=1}^{N}\mathbf{X}_{t_r}^{l} \\
\hat{C}_{A,t_r} &= \frac{1}{N-1}\sum_{l=1}^{N}\left(\mathbf{X}_{t_r}^{l}-\hat{\mu}_{A,t_r}\right)\left(\mathbf{X}_{t_r}^{l}-\hat{\mu}_{A,t_r}\right)^{T} \\
\mathbf{z}_{t_r}^{l} &= g(\mathbf{X}_{t_r}^{l}) \quad l=1,\ldots,N \\
\hat{\mathbf{z}}_{A,t_r} &= \frac{1}{N}\sum_{l=1}^{N}\mathbf{z}_{t_r}^{l} \\
\hat{C}_{ZZ} &= \frac{1}{N-1}\sum_{l=1}^{N}\left(\mathbf{z}_{t_r}^{l}-\hat{\mathbf{z}}_{A,t_r}\right)\left(\mathbf{z}_{t_r}^{l}-\hat{\mathbf{z}}_{A,t_r}\right)^{T}+R \\
\hat{C}_{XZ} &= \frac{1}{N-1}\sum_{l=1}^{N}\left(\mathbf{X}_{t_r}^{l}-\hat{\mu}_{A,t_r}\right)\left(\mathbf{z}_{t_r}^{l}-\hat{\mathbf{z}}_{A,t_r}\right)^{T} \\
K_k &= \hat{C}_{XZ}\hat{C}_{ZZ}^{-1} \\
\mu_{X,t_r} &= \hat{\mu}_{A,t_r}+K_k\left(\mathbf{z}_{t_r}-\hat{\mathbf{z}}_{A,t_r}\right) \\
C_{X,t_r} &= \hat{C}_{A,t_r}-K_k\hat{C}_{ZZ}K_k{}^{T}
\end{aligned}
\tag{16}
$$

The estimation procedure followed by the hybrid filter 2 while outside the FOV and during the PF to UKF transition is similar to that of an EnKF [5, 10] i.e., using an ensemble of particles to perform uncertainty propagation and a Kalman measurement update for data assimilation. The Kalman measurement update enables the EnKF to keep the number of particles small even in high dimensional estimation problems. However, unlike hybrid filter 2, the EnKF performs the Kalman update on individual particles to obtain samples from the posterior PDF directly. Given an ensemble of states $\psi = [\mathbf{X}_1, \mathbf{X}_2, \cdots, \mathbf{X}_n]$, corresponding measurement vectors $\phi = [h(\mathbf{X}_1), h(\mathbf{X}_2), \cdots, h(\mathbf{X}_n)]$ and a recorded measurement $\mathbf{y}$, the ensemble Kalman update is given by

$$\hat{\boldsymbol{\psi}} = \boldsymbol{\psi} + K_k(\mathbf{Y}-\boldsymbol{\phi}),$$

where Y is the matrix of perturbed observations.

$$
\begin{aligned}
Y &= [\mathbf{y}^1, \cdots, \mathbf{y}^n], \quad \mathbf{y}^i = \mathbf{y} + \boldsymbol{\nu}^i \\
\boldsymbol{\nu}^i &\sim \mathcal{N}(0, R).
\end{aligned}
$$

The posterior ensemble $\hat{\boldsymbol{\psi}}$ is then used for propagation in the next time step. In contrast, the transition equations described in hybrid filter 2 computes the posterior

mean and covariance directly from the statistics of the propagated state variable. An important advantage of this hybrid update is that it allows the number of particles to be varied during the filtering process. This is not possible in a standard EnKF in which the size of the ensemble is fixed at the beginning of the simulation.

Hybrid Filter 3

The PF to UKF transition in hybrid filter 3 is also accomplished through a Kalman measurement update. However, unlike hybrid filter 2, it uses the UT to compute the Kalman gain and perform the mean and covariance update. To start with, it uses the ensemble averaged mean $\hat{\mu}_{A,t_r}$ and covariance $\hat{C}_{A,t_r}$ of the state vector to compute sigma points as given by Eq. 10. Then the sigma points are used to compute the terms $\hat{\mathbf{z}}$, $\hat{C}_{ZZ}$ and $\hat{C}_{XZ}$ with UT. The Kalman gain is computed using these matrices as $K_k = \hat{C}_{XZ}\hat{C}_{ZZ}^{-1}$. The transition is completed by evaluating the expressions for μ_{X,t_r} and C_{X,t_r} in Eq. 16 with these terms.

Effect of Transition Design

The following simulation was conducted to study the effect of different transition schemes on the posterior uncertainty estimate. A set of 1000 particles is sampled from an initial Gaussian PDF. The initial uncertainty in position is set to 1 km and that in velocity is set to 10 m/s along each direction. The particles are then propagated forward through 100 time steps with $\Delta t = 1s$. At this point, the first measurement $\mathbf{z}$ is registered and the moments of the posterior random variable are computed using the three different transition schemes. The 3-sigma ellipses of the posterior marginal distribution in X-Y coordinates computed using the three PF-UKF transition designs are presented in Fig. 3a. The posterior covariance computed by propagating the initial Gaussian PDF with a UKF is also included for comparison. The covariance computed using hybrid filter 1 is seen to be the smallest among the four. This happens when the measurement likelihood drops considerably over short distances as a result of which a large section of the particles acquire negligible weights. The contribution of these particles to the posterior covariance estimate also reduces on account of their diminished weights. While it is true that one can employ a relatively small number of particles for estimation outside the FOV, as there are no measurements, relying on the particle measurement update during PF to UKF transition seems to once again bring about the curse of dimensionality. This indicates that the feasibility of a UKF-PF hybrid filter that uses a small number of particles without the risk of depletion as conceived in the section "The Unscented Kalman-Particle Hybrid Filter" depends on the PF to UKF transition design. Transition design 1 employs the particle measurement update and is prone to underestimating the posterior covariance unless a sufficiently large particle ensemble is used.

The risk of covariance collapse is averted when the transition is performed through a Kalman update on the ensemble. As Fig. 3a indicates, the posterior covariance estimates provided by transition designs 2 and 3 are much larger in comparison to that

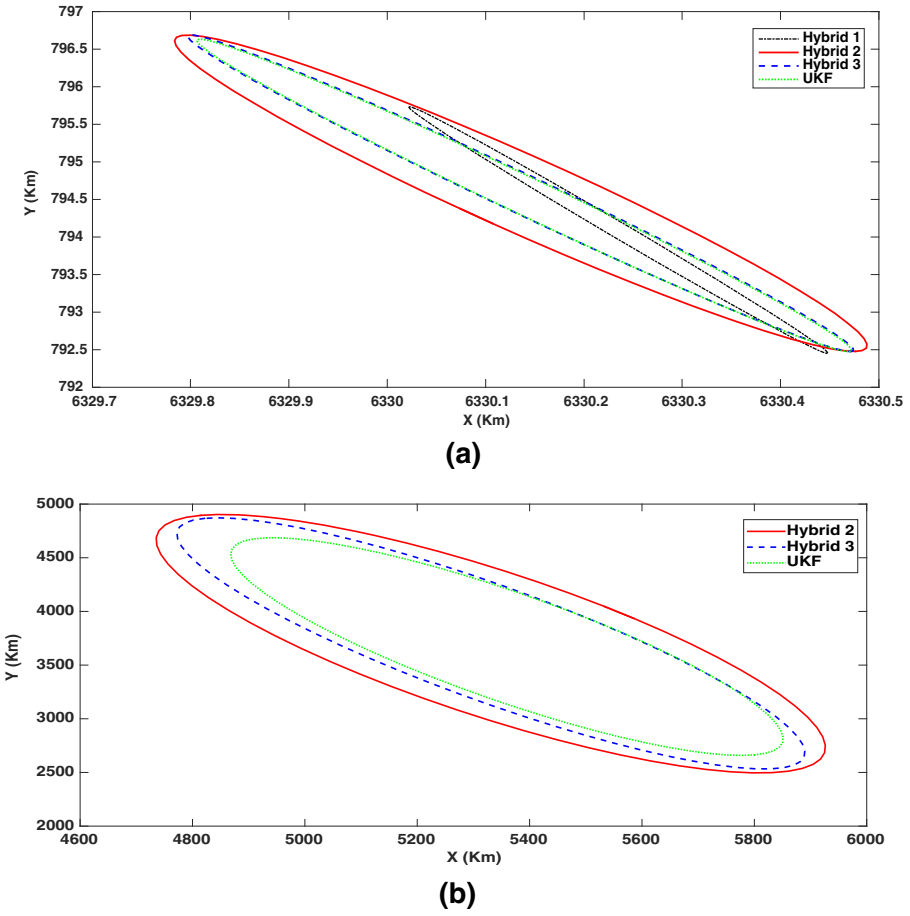

Fig. 3 Effect of transition design on the estimated uncertainty (C_{X_t}) in posterior PDF

estimated by design 1. Transition designs 2 and 3 are not subject to the problem of weight depletion as they do not rely on measurement likelihoods to perform the update. In this case, the covariance estimated by the UKF is seen to be similar in size to that estimated by hybrid filters 2 and 3. However, on raising the initial uncertainty in velocity to 1 km/s and increasing the simulation time to 500 time steps, the uncertainty estimated using the UKF is seen to be distinctly smaller than that obtained from hybrid filters 2 and 3. This is shown in Fig. 3b. The hybrid filter 1 is observed to undergo complete covariance collapse in this case. Hence, it is not included in Fig. 3b. It clearly appears that, by transitioning from PF to UKF through a Kalman update, the problem of particle depletion and subsequent covariance collpase can be avoided. A general algorithm for implementing the UKF-PF hybrid filter is presented in Algorithm 1.

Dynamics & Measurement Models

This section contains a brief description of the perturbed dynamics of orbiting objects. Following this, an angles-only measurement model, employed to aid state estimation, is described.

Algorithm 1 UKF-PF Hybrid filter for space object tracking

S_1 : PDF in functional form (inside FOV),
S_2 : PDF as ensemble (outside FOV),
$C(X)$: Boundary of FOV,
P_d : Probability of detection.
Initialize: $P(X) = P_0(X)$, $S = S_0$
At t_k

if $S = S_1$ **then**
  if $C(X_k) <= 0$ **then**
    Use UKF
    SET $S = S_1$
  else
    SAMPLE FROM P(X)
    USE PF
    SET $S = S_2$
  end if
else
  if $C(X_k) <= 0$ $\eta > \eta_0$ **then**
    EXECUTE PF-UKF TRANSITION
    COMPUTE P(X)
    SET $S = S_1$
  end if
else
  USE PF
  SET $S = S_2$
end if

Dynamics of Space Objects

The acceleration experienced by an object, of mass m_o in the inverse square gravitational field of Earth is given by

$$\mathbf{a_g} = -\frac{GM_e m_o \mathbf{r}}{r^3}. \tag{17}$$

Here G is the universal gravitational constant, $\mathbf{r}$ the vector joining the center of Earth to the center of mass (CM) of the object, r its magnitude and M_e the mass of Earth. The gravitational acceleration, as given in Eq. 17, assumes that the central body is spherically symmetric. In reality, the Earth has a non-symmetric mass distribution similar to an oblate ellipsoid, with more mass distributed along the equator.

To account for the non-sphericity, the gravitational potential is expanded into a series of spherical harmonics. The dominant perturbation term in the resulting expansion is called the J_2 harmonic. The perturbing acceleration arising from the J_2 term, $\mathbf{a_{J_2}}$ is given by

$$\mathbf{a_{J_2}} = -\frac{3}{2} J_2 \frac{GM_e}{r^2} \left(\frac{r_{eq}}{r}\right)^2 \begin{bmatrix} (1 - 5(\frac{x_3}{r})^2)\frac{x_1}{r} \\ (1 - 5(\frac{x_3}{r})^2)\frac{x_2}{r} \\ (3 - 5(\frac{x_3}{r})^2)\frac{x_3}{r} \end{bmatrix}, \tag{18}$$

where r_{eq} is the equatorial radius of the Earth and x_1, x_2, x_3 are the Cartesian coordinates of the CM of the object measured from the center of Earth [20]. In addition to this, the orbital motion is also affected by the non-conservative atmospheric drag which may be significant in low Earth orbits. Assuming a blunt form factor, the acceleration due to atmospheric drag force can be computed as

$$\mathbf{a_D} = -\left(\frac{A_{cs}}{m_o}\right) \rho C_d \left(\frac{v^2}{2}\right) \mathbf{i_v}. \tag{19}$$

Here A_{cs} is the cross sectional area of the object, C_d, the drag coefficient, and ρ the atmospheric density. The term v represents the magnitude of relative velocity between atmosphere and orbiting object whereas $\mathbf{i_v}$ is the unit vector along its direction. A simple exponential model may be employed to describe the variation of atmospheric density with altitude, according to which

$$\rho(r) = \rho_0 \exp\left(-\left(\frac{r - r_0}{H}\right)\right). \tag{20}$$

Here ρ_0 and r_0 are reference density and radius. The variable H, known as scale height, is the vertical distance over which the density of the atmosphere reduces by a factor of mathematical constant e. The resultant acceleration experienced by the object is then given by

$$\ddot{\mathbf{r}} = \mathbf{a_g} + \mathbf{a_{J_2}} + \mathbf{a_D}. \tag{21}$$

In this study we have ignored the effects of other forces such as third body perturbations since we consider only space objects in low Earth orbits (LEO). The perturbation terms present in the resultant acceleration force the object to undergo full three dimensional motion. Hence the state of the system is taken to be

$$\mathbf{X} = [x_1 \; x_2 \; x_3 \; \dot{x_1} \; \dot{x_2} \; \dot{x_3}]^T. \tag{22}$$

where x_1, x_2, x_3 are the Cartesian coordinates of the object measured with respect to an inertial frame placed at the center of earth. In practice, we integrate Eq. 21, which describes a continuous time dynamical system, numerically with fixed time steps Δt. This allows us to obtain an approximate discrete time solution $f(\mathbf{X}_t)$ which maps the state $\mathbf{X}_t$ at time t to that at $t + \Delta t$, i.e., $\mathbf{X}_{t+\Delta t}$. In addition to the acceleration terms described in the Eq. 21, a sequence of independent and normally distributed noise terms are added in the state update equations to account for modeling uncertainties. However, as mentioned in "Problem Statement", we assume the process noise in the space object tracking problem to be minimal. Therefore, the process noise terms are sampled as acceleration terms drawn from a zero mean Gaussian PDF with covariance $10^{-18} I_3$.

Measurement Model

Let $\mathbf{r}$ and $\mathbf{r_s}$ be the inertial position vectors of the space object O and the ground station respectively. Then the relative position of the object with respect to the ground station is given by

$$\mathbf{r^i} = \mathbf{r} - \mathbf{r_s}. \tag{23}$$

The sensor measures the topocentric inclination (θ) and right ascension (ϕ) from a ground station assumed to be located on the Earth's equator. The coordinatization of the relative position vector of the space object with respect to the ground station, in the station frame, may be computed by multiplying the inertial vector $\mathbf{r^i}$ with the appropriate orthonormal transformation matrix. If the effects due to precession, nutation etc. of the Earth are neglected, then the ground station is in an elemental rotation about the polar axis with respect to the inertial frame. At $t = 0$, both ground frame and inertial frame are aligned. Assuming a constant spin rate ω for the Earth, the transformation matrix for the ground station at time t may be calculated as

$$F(t) = \begin{bmatrix} \cos\omega t & \sin\omega t & 0 \\ -\sin\omega t & \cos\omega t & 0 \\ 0 & 0 & 1 \end{bmatrix}. \tag{24}$$

If $[r_x^i \; r_y^i \; r_z^i]$ are the Cartesian coordinates of the object in the ground frame, then θ and ϕ are calculated as

$$\theta = \sin^{-1}\left(\frac{r_z^i}{r^i}\right) \tag{25}$$

$$\phi = \tan^{-1}\left(\frac{r_y^i}{r_x^i}\right) \tag{26}$$

where $r^i = \sqrt{{r_x^i}^2 + {r_y^i}^2 + {r_z^i}^2}$.

A zero mean Gaussian measurement noise with 3.9 arcsec standard deviation is assumed. The FOV of the ground station is limited by 75 degrees on either side in the azimuthal direction and by 90 degrees on either side in the polar direction. An illustration of the space object-ground station system is presented in Fig. 4. Once the space object is inside the FOV of the sensor, measurements are registered with a preset probability of detection P_d. It must be noted here that the P_d is a state independent factor employed solely for the purpose of ensuring that the measurements are not recorded at all instants and that they come in at random even when the object is within the FOV.

Simulations and Results

In this section, the UKF-PF hybrid filtering framework is applied to two test case problems of space objects in low Earth orbits (LEO). The three hybrid filter variants are simulated along with standard implementations of UKF and PF to compare

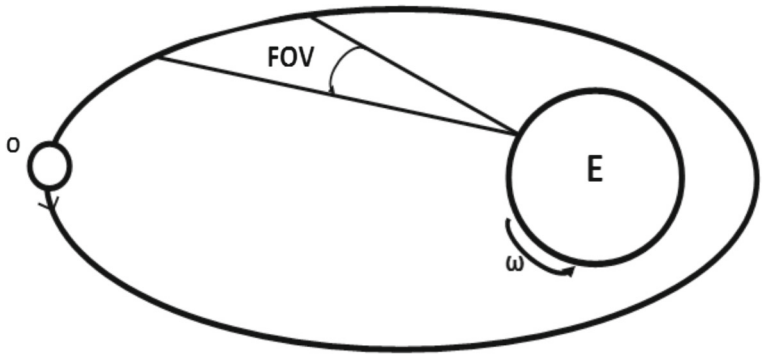

Fig. 4 The sensor is fixed on the ground station which defines a non inertial frame that spins with the earth

the estimation performance. The estimation results are assessed for accuracy and consistency.

The accuracy of the estimator is evaluated in terms of the root mean squared error (RMSE) in position estimates. The RMSE in position estimate at time t may be calculated as

$$RMSE_{position} = \sqrt{\frac{1}{N_{Mo}} \sum_{i=1}^{N_{Mo}} \sum_{j=1}^{3} (x'_{j,t,i} - X_{j,t,i})^2}. \tag{27}$$

Here N_{Mo} represents the number of Monte Carlo runs over which the RMSE is computed. The terms $x'_{j,t,i}$ and $X_{j,t,i}$ represent the actual and estimated position coordinates of the object at time t in the direction j during the i^{th} Monte Carlo run. Smaller RMSE values represent more accurate estimates.

The normalized estimation error squared (NEES) test is employed to evaluate the consistency of estimates [3]. The NEES test is performed by computing the normalized residual $\beta_{t,i}$, which is defined as

$$\beta_{t,i} = (\mathbf{x}'_{t,i} - \mathbf{X}_{t,i})^T {C_{X,t,i}}^{-1} (\mathbf{x}'_{t,i} - \mathbf{X}_{t,i}). \tag{28}$$

Here $\mathbf{x}'_{t,i}$ represents the actual state occupied by the object at time t in the i^{th} Monte Carlo run. If $\mathbf{X}_{t,i} \in \mathbb{R}^n$ is distributed according to a Gaussian PDF, then $\beta_{t,i}$ is a chi-square random variable with expected value n. To assess the consistency of the hybrid filter, the average NEES test statistic computed over multiple Monte Carlo runs is considered. The average NEES test statistic for the estimates at time t computed over N_{Mo} simulations is given by

$$\beta_t = \frac{1}{N_{Mo}} \sum_{i=1}^{N_{Mo}} \beta_{t,i}. \tag{29}$$

When the state vector is a six dimensional Gaussian random variable, the sum $N_{Mo}\beta_t$ can be shown to be distributed according to a χ^2 density with $6N_{Mo}$ degrees of freedom. Consequently, the consistency of the estimator may be tested by examining whether β_t falls within probable bounds computed from the corresponding χ^2 distribution. When the average NEES is computed over 50 Monte Carlo runs, a 99.5% probability upper bound for the random variable β_t is found to $Ub_{0.995} = 7.3369$. If β_t assumes a value above 7.3369, then the covariance estimates are inconsistent with the estimation errors, i.e., it is likely that the covariances $C_{X,t,i}$ are underestimated. In other words, the estimates are optimistic.

Case 1 In this test case, the estimated initial state of the object is set at

$$\mathbf{X}_0 = \left[\, 7800 \;\; 0 \;\; 0 \;\; 0 \;\; 6.8443\cos(\pi/4) \;\; 6.8443\sin(\pi/4) \,\right]^T, \tag{30}$$

where the lengths and speeds are in km and km/s respectively. This is a 45° inclined LEO with a period of 6080 s and eccentricity of 0.0833. The uncertainty in the initial state estimate is characterized by a standard deviation of 1 km in position estimates and 1 m/s in velocity estimates. The probability of detection is set at 0.9. The filters are employed to estimate the state of the space object for a total duration of 24 hours. In hybrid filter simulations, the number of particles used during the sequential Monte Carlo update is set at 500. A sequential importance resampling (SIR) filter is used as the standard PF implementation [2]. In order to maintain uniform computational costs, the SIR is also implemented with 500 particles. The simulations for test case 1 are repeated over 50 Monte Carlo runs and the averaged values for NEES and RMSE are computed. The estimation results for the hybrid filters and the UKF for test case 1, are plotted in Fig. 5. In Fig. 5a the RMSE in position for each filter are plotted against time. As the objects are initialized inside the FOV, the uncertainty in position estimates are observed to diminish sharply in the beginning.

Once the object moves out of the FOV, measurements become unavailable, errors accumulate and the amount of uncertainty increases steadily as signified by the upswing in the $RMSE_{position}$ plots. However, after reentry into the FOV, more information is added with each recorded measurement and the magnitude of RMSE drops again. This pattern repeats over the many subsequent FOV entries and exits. All four filters follow this trend and showcase similar performance, as seen in Fig. 5a. For the three hybrid filters and the UKF, the error in position estimates during the last four hours of the simulated time are seen to be of the order of 10^0m.

Figure 5b shows the results of NEES test for hybrid filter 1 and the UKF for test case 1. A horizontal line indicating $y = Ub_{0.995}$ has been included for reference. It is seen that the estimates generated by hybrid filter 1 and UKF are inconsistent for a very long time. Comparing the NEES plots of hybrid filter 1 and UKF with their corresponding RMSE plots reveals the following. In the case of UKF, once the object exits the FOV, the estimation error and the value of NEES test statistic are both seen to grow. The NEES test statistic is seen to overstep the $Ub_{0.995}$ line during this stage. This indicates that when the object is outside the FOV, the covariance estimated by the UKF does not grow fast enough to ensure that the estimates remain consistent. However, the value of UKF NEES test statistic is seen to drop once the measurements start to reappear. In contrast, the hybrid filter 1 estimates are seen to remain consistent

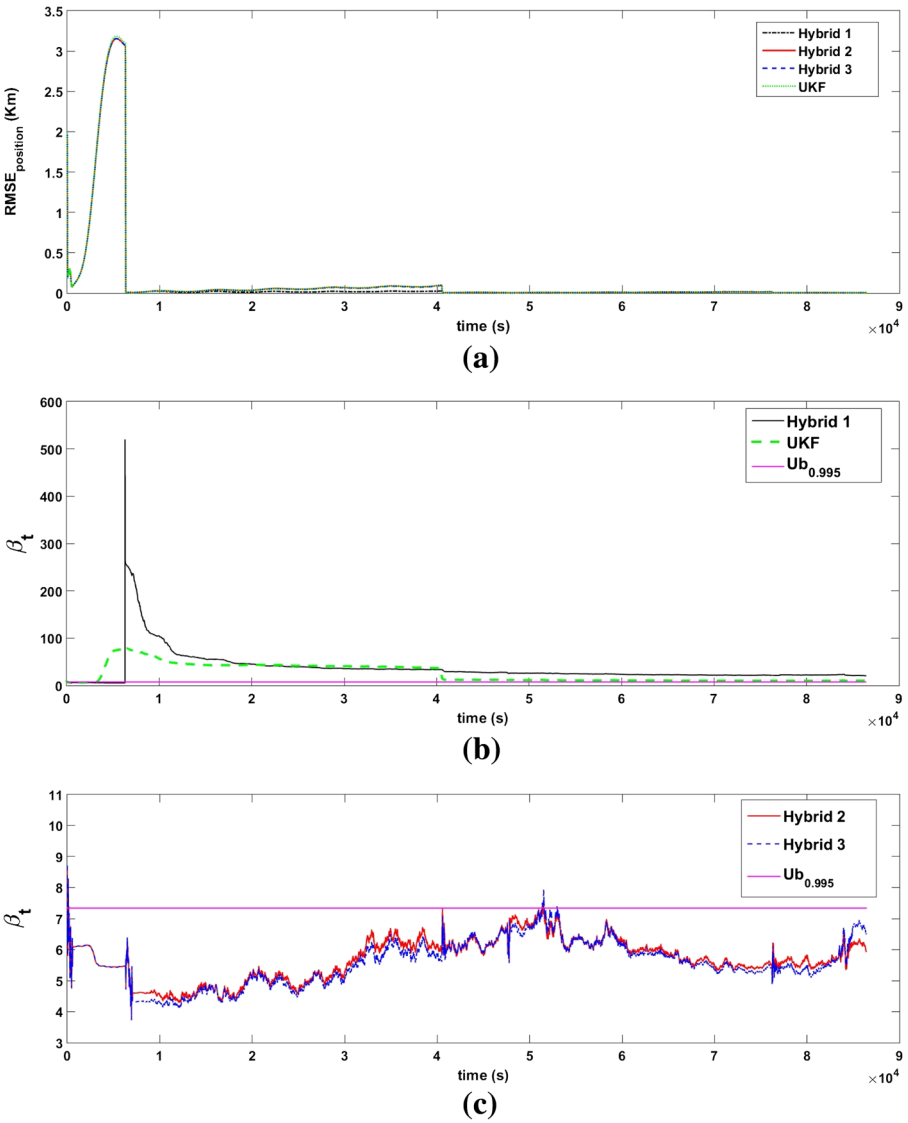

Fig. 5 Test case 1 results: **a** $RMSE_{position}$ **b** NEES Plot 1 **c** NEES Plot 2

throughout the flight of the Object outside the FOV until the first re-entry. The NEES plot of hybrid filter 1 crosses the $Ub_{0.995}$ only when the measurements reappear and the PF to UKF transition is triggered. As mentioned before, hybrid filter 1 relies on the particle measurement update which is prone to underestimating the posterior uncertainty. As a result, the NEES test statistic is seen to spike during the transition. The NEES test results for the hybrid filters 2 and 3 are plotted in Fig. 5c. The results

show that estimates provided by hybrid filters 2 and 3 remain consistent during most of the simulated time.

The performance of the filters in NEES test may be compared using the fraction of the total simulated time period during which each filter generated consistent estimates. The fraction of times during which the hybrid filters and the UKF provided estimates that lie within the 99.5% bounds in test case 1 are plotted in Fig. 6. It is seen that estimates provided by hybrid filter 2 and 3 are consistent during 99.84% and 99.69% of the simulated time in test case 1. Estimates provided by the hybrid filter 1 are seen to be consistent during 7.28% of the simulated time. The consistency fraction for the UKF in test case 1 is found to be 3.69%. This indicates that UKF and hybrid filter 1 are prone to underestimating the posterior covariance, even though the estimation errors committed by all four filters are similar.

When it was employed with 500 particles to estimate the test case 1, the covariance of the SIR filtered is observed to collapse within a few time steps. The small process noise and accurate measurements result in loss of diversity of the ensemble at each resampling step. Consequently, the sample covariance becomes negligible in a few time steps when the actual estimation errors are significant. As a result, the value of β_t for the SIR filter is found to quickly blow up. It may well be possible to perform estimation of a six dimensional nonlinear system using an SIR filter when implemented with a much larger number of particles. However increasing the number of particles to prevent weight depletion will also increase the computational cost. It is notable that the hybrid filters 2 and 3 offer reliable performance in this six dimensional estimation problem while requiring only a relatively small number of particles.

Case 2 In this case, the estimated initial state of the object is set to

$$\mathbf{X}_0 = \left[\, 6800 \;\; 0 \;\; 0 \;\; 0 \;\; 7.5989\cos(\pi/3) \;\; 7.5989\sin(\pi/3) \,\right]^T . \tag{31}$$

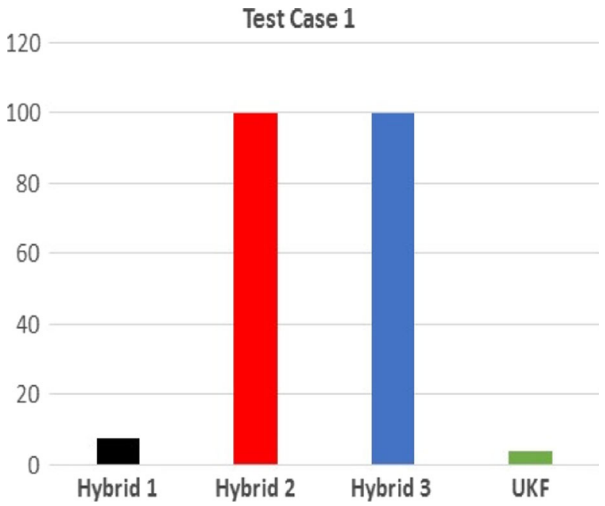

Fig. 6 Consistency of estimates in test case 1

This is a 60° inclined low Earth orbit with a time period of 5580.5s. The initial uncertainty in position is increased to 3 km along each direction and that in velocity is raised to 1 km/s. The probability of detection is reduced to 0.4. As mentioned before, for space objects, the growth in uncertainty is remarkably sensitive to the initial uncertainty in velocity. When the uncertainty is larger and state PDF is more diffuse, the accumulation of errors due to linearization also becomes much more

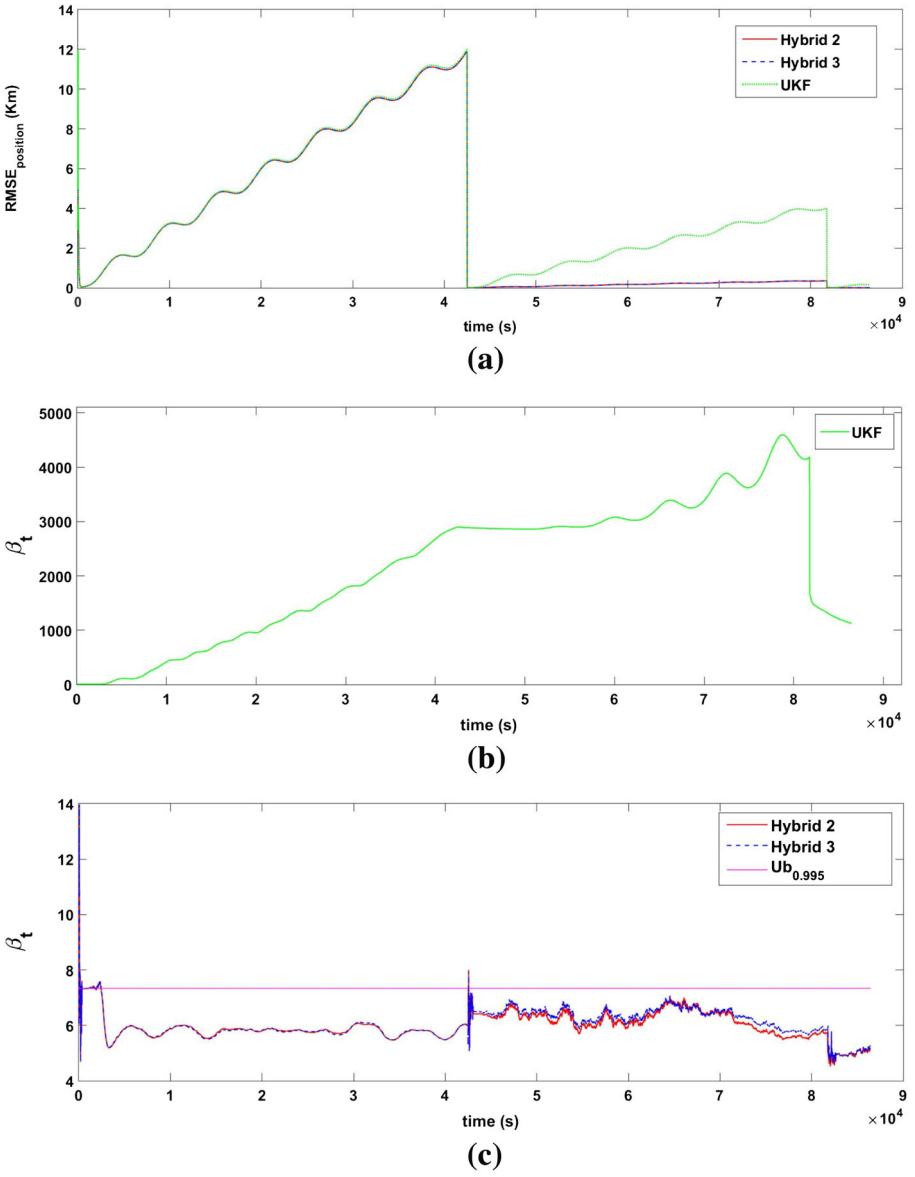

Fig. 7 Test case 2 results: **a** $RMSE_{position}$ **b** NEES Plot 1 **c** NEES Plot 2

severe. The nonlinearity induced distortion of state PDF is also larger in such a case. Case 2 is used to test the performance of the hybrid filters under such conditions.

The simulation was conducted for a period of 24 hrs. The results, averaged over 50 Monte Carlo runs, are given in Fig. 7. The estimation results for hybrid filter 1 in test case 2 are not presented as it was observed to undergo covariance collapse due to significant particle depletion. The SIR filter is also observed to undergo covariance collapse in test case 2.

The $RMSE_{position}$ plots given in Fig. 7a indicate that for all three filters, the errors in position estimates quickly drop in the beginning since measurements are recorded. Once the object exits the FOV, the errors start to grow. The errors shrink again when the object reenters the FOV of the sensor and a new batch of measurements become available.

From Fig. 7a it can be observed that the estimation errors committed by UKF in test case 2 are seen to be much worse than that by hybrid filters 2 and 3. For hybrid filters 2 and 3, the errors in position estimates during the final four hours of the simulated time are seen to be of the order of 10^{-1} Km. For UKF, this number is seen to be of the order of 10^{0} km. The NEES test results for the UKF estimates in test case 2 are plotted in Fig. 7b. The results indicate that the UKF estimates are inconsistent during most of the simulated time. By comparing Fig. 7b with Fig. 7a, it can be observed that the value of UKF NEES test static grows as the estimation error increases. Once the $Ub_{0.995}$ is overstepped, the UKF estimates stay inconsistent for the entire length of the remaining simulation time, in spite of recording several additional measurements. The NEES test results for hybrid filters 2 and 3 are plotted in Fig. 7c. The hybrid filters 2 and 3 are seen to produce consistent estimates during 98.41 and 98.49% of the times respectively. In contrast, the UKF estimates are consistent during only 2.74% of the total simulation time. The fraction of the simulated time during which each filter offered consistent estimates is plotted in Fig. 8.

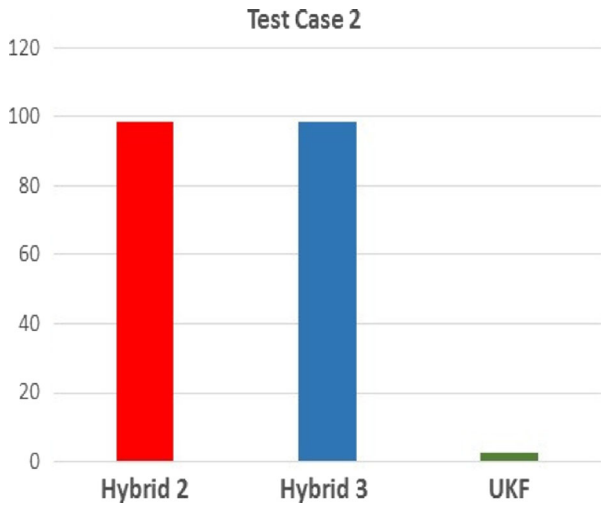

Fig. 8 Consistency of estimates in test case 2

Conclusions

The design and application of a hybrid UKF-PF based estimation framework for tracking space objects has been presented. The dynamics of space objects under the effects of J_2 perturbation and atmospheric drag is considered. Conventionally employed nonlinear filters such as EKF and UKF are not effective in estimation problems in which the state PDF is distorted under nonlinear transformations for extended periods. Even though the particle filter does not enforce restrictive assumptions on the nature of PDF, its implementation becomes computationally expensive as the dimensionality of the state space increases.

The proposed hybrid filtering framework employs the UKF for tracking when the target is inside the FOV of the observer. In order to handle the nonlinear distortion outside the FOV, the tracking scheme transitions from UKF to PF as the object exits the FOV. The hybrid filter addresses the problem of particle depletion through a suitably designed PF to UKF transition scheme based on a Kalman update. The hybrid filtering scheme was employed to estimate the state of a space object in inclined low Earth orbits and the estimation performance is studied in terms of the RMSE and NEES metrics. Hybrid filters that employed a Kalman measurement update for executing the PF to UKF transition were observed to consistently match or outperform the UKF in terms of accuracy and consistency of estimates. It is observed that UKF based estimates often become inconsistent as the estimation errors grow outside the FOV. State estimation using the SIR filter was found to be unsuccessful when implemented with the same number of particles as the hybrid filters. The hybrid filters that employed the Kalman measurement update are found to offer reliable estimation performance even with large initial uncertainty and sparse measurements while using a relatively small number of particles. Based on the results obtained here, a general multimodal nonlinear filter named Particle Gaussian Mixture (PGM) Filter has been proposed by the authors [18]. The PGM filter employs a particle approximation for propagation and a Kalman update of the type employed in hybrid filter 2 or 3 for measurement update. Additionally, it does not require the assumption 2 enforced on process noise.

References

1. Alspach, D., Sorenson, H.: Nonlinear bayesian estimation using gaussian sum approximations. IEEE Trans. Autom. Control **17**(4), 439–448 (1972)
2. Arulampalam, S., Maskell, S., Gordon, N., Clapp, T.: A tutorial on particle filters for online nonlinear/non-gaussian bayesian tracking. IEEE Trans. Signal Process. **50**(2), 174–188 (2001). doi:10.1109/78.978374
3. Bailey, T., Nieto, J., Guivant, J., Stevens, M., Nebot, E.: Consistency of the Ekf-Slam Algorithm. In: Proceedings of the 2006 IEEE/RSJ International Conference on Intelligent Robots and Systems, pp. 3562–3568 (2006). doi:10.1109/IROS.2006.281644
4. Bengtsson, T., Bickel, P., Li, B.: Curse-of-dimensionality revisited: collapse of particle filter in very large scale systems. In: Probability and Statistics: Essays in Honor of David A. Freedman, vol. 2, pp. 316–334 (2008)
5. Burgers, G., Leeuwen, P.V., Evensen, G.: Analysis scheme in the ensemble kalman filter. Mon. Weather. Rev. **126**(6), 1719–1724 (1998)

6. Daum, F.: Nonlinear filters beyond the kalman filter. IEEE Aerosp. Electron. Syst. Mag. **20**(8), 57–69 (2005). doi:10.1109/MAES.2005.1499276
7. Daum, F., Huang, J.: Curse of dimensionality and particle filters. In: Proceedings of IEEE Aerospace Conference, pp. 1979–1993 (2003). iSBN:0-7803-7651-X
8. DeMars, K., Bishop, R., Jah, M.: Entropy-based approach for uncertainty propagation of nonlinear dynamical systems. J. Guid. Control. Dyn. **36**(4), 1047–1056 (2013). doi:10.2514/1.58987
9. Doucet, A.: On Sequential Monte Carlo Methods for Bayesian Filtering. Tech. Rep. CUED/F-INFENG/TR.310, Dept. Eng., Univ. Cambridge (1998)
10. Evensen, G.: Sequential data assimilation with a nonlinear quasigeostrophic model using monte carlo methods to forecast error statistics. J. Geophys. Res. Oceans **99**(C5), 10 143–10 162 (1994)
11. Gordon, N., Salmond, D., Smith, A.: A novel approach to nonlinear/non-gaussian bayesian state estimation. IEEE Proceedings F, Radar and Signal Processing **140**(2), 107–113 (1993). doi:10.1049/ip-f-2.1993.0015
12. Julier, S.J., Uhlmann, J.K.: Unscented filtering and nonlinear estimation. In: Proceedings of the IEEE, vol. 92, pp. 401–402 (2004). doi:10.1109/JPROC.2003.823141
13. Julier, S.J., Uhlmann, J.K., Durrant-Whyte, H.: A new approach for filtering nonlinear systems. In: Proceedings of the American Control Conference, pp. 1628–1632 (1995). iSBN:0-7803-2445-5
14. Kalman, R.E.: A new approach to linear filtering and prediction problems. Trans. ASME J. Basic Eng. **82**(1), 35–45 (1960). doi:10.1115/1.3662552
15. Kalman, R.E., Bucy, R.S.: New results in linear filtering and prediction theory. Trans. ASME J. Basic Eng. **83**(1), 95–108 (1961). doi:10.1115/1.3658902
16. Kalnay, E., Li, H., Miyoshi, T., Ballabrera-Poy, J.: 4-D-var or ensemble kalman filter? Tellus A **59**(5), 758–773 (2007)
17. Psiaki, M.L.: The blind tricyclist problem and a comparative study of nonlinear filters. IEEE Control. Syst. Mag. **33**(3), 40–54 (2013)
18. Raihan, D., Chakravorty, S.: Particle gaussian mixture (Pgm) filters. In: Proceedings of the 2016 19Th International Conference on Information Fusion (FUSION), pp. 1369–1376 (2016). iSBN:978-0-9964-5274-8
19. Ristic, B., Arulampalam, S., Gordon, N.: Beyond the Kalman Filter: Particle Filters for Tracking Applications. Artech House, Boston, London (2004). iSBN:158053631X
20. Schaub, H., Junkins, J.: Analytical Mechanics of Space Systems. AIAA, Reston VA (2003). iSBN:1624102409
21. Smith, G., Schmidt, S., McGee, L.: Application of statistical filter theory to the optimal estimation of position and velocity on board a circumlunar vehicle. Tech. Rep. NASA TR-135, NASA (1962)
22. Sorenson, H., Alspach, D.: Recursive bayesian estimation using gaussian sums. Automatica **7**(4), 465–479 (1971). doi:10.1016/0005-1098(71)90097-5
23. Terejanu, G., Singla, P., Singh, T., Scott, P.: Adaptive gaussian sum filter for nonlinear bayesian estimation. IEEE Trans. Autom. Control **56**(9), 2151–2156 (2011). doi:10.1109/TAC.2011.2141550
24. Wan, E., van der Merwe, R.: The Unscented Kalman Filter. In: Haykin, S. (ed.) Kalman Filter and Neural Networks, pp. 221–280. Wiley, New York (2001). iSBN:9780471369981
25. Whitaker, J., Hamill, T.: Ensemble data assimilation without perturbed observations. Mon. Weather. Rev. **130**(7), 1913–1924 (2002)